



# OPEN Removal of methylene blue from synthetic industrial wastewater by using geopolymer prepared from partially dealuminated metakaolin

Khaled Elewa<sup>1</sup>, A. F. Tawfic<sup>2</sup>✉, Mostafa Tarek<sup>1</sup>, Nabil Abdullah Al-Sagheer<sup>3</sup> & Nabil M. Nagy<sup>1</sup>

Industrial wastewater frequently contains a huge of pollutants, such as heavy metals, dyes, and organic compounds, leading to considerable environmental discharge. Methylene Blue (MB), a cationic dye extensively utilized in the textile and pharmaceutical sectors, presents significant hazards to aquatic environments and human health. Exposure to MB may result in negative effects, including dermal irritation, stomach discomfort, and possible long-term ecological consequences. This research investigates the elimination of MB from synthetic industrial wastewater utilizing a geopolymer derived from Partially De-aluminated Metakaolin (PDK) by using adsorption technique it is a simple, low-cost, and effective method for removing a variety of pollutants. The geopolymeric materials were analysed using XRF, XRD, FTIR, SEM, EDX, and BET to confirm its structure then used for MB removal. The specific surface area of the geopolymer was determined to be 9.3 m<sup>2</sup>/g and a pore volume of 0.024 m<sup>3</sup>/g. Its kinetics and isotherms were investigated in the MB dye adsorption experiments. The adsorption was influenced by dose, initial dye concentration, pH, and contact time. According to the results, the maximum adsorption capacity (8 mg/g) was attained at 60 mg/L MB, 60 min of contact time, and pH 7–12 for one hour. The experimental data indicated that Freundlich isotherm model was the best-fit model to describe the sorption of MB on the synthesised geopolymer with higher determination coefficients R<sup>2</sup> of 0.996. Value of n greater than unity indicates a favourable adsorption taking place. This indicated that the adsorption occurs under a multilayer and heterogeneous surface for MB. The adsorption kinetics of MB onto GP was investigated using pseudo first order, and pseudo second order models as shown in, using the experimental data at various initial concentrations. The calculated parameters values obtained from the application of three models are tabulated. By comparing R<sup>2</sup> for each applied model and the compatibility between the estimated and observed q<sub>e</sub> values, the most favourable model may be identified. The pseudo 2<sup>nd</sup> order R<sup>2</sup> value are greater than other models.

**Keywords** Adsorption, Geopolymer, Industrial wastewater treatment, Metakaolin, Methylene blue removal, Silicious waste of aluminum sulfate-based kaolin

The treatment of effluents has become a difficult problem in environmental sciences as a result of the rapid industrial growth that has caused the discharge of many colours into the aquatic environment. The extensive use of dyes across various sectors, including textiles, leather, additives, petroleum products, paper, cotton, wool, plastics, and pharmaceuticals, has led to increased water pollution from colorants, garnering the attention of the scientific community.<sup>1–4</sup> Dyes are utilized on substrates to give them a persistent coloration that withstands fading from exposure to water, light, oxidizing chemicals, perspiration, and microbiological assault<sup>5–7</sup>. Owing to these benefits, a variety of dyes are employed across numerous industries, including textiles, food, rubber, printing, cosmetics, pharmaceuticals, plastics, concrete, and paper, for diverse applications<sup>8–11</sup>. These companies produce significant volumes of wastewater filled with carcinogenic and poisonous dyes, rendering the water unsuitable for human consumption<sup>12</sup>. Methylene blue (MB), one of the most used industrial dyes, it has a molecular weight and chemical formula of 319.85 g/mol and C<sub>16</sub>H<sub>18</sub>N<sub>3</sub>Sl (Fig. 1), is a basic dye that is utilized in many different industries, including color photography, textile dyeing, and the petroleum sector. For this reason,

<sup>1</sup>Department of Civil Engineering, Military Technical College, Cairo, Egypt. <sup>2</sup>Head of Nuclear Engineering Department, Military Technical College, Cairo, Egypt. <sup>3</sup>Aluminum Sulfate Co. of Egypt, Cairo, Egypt. ✉email: Tawficaf@mtc.edu.eg

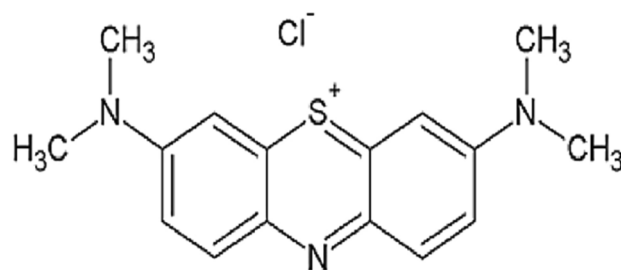


**Fig. 1.** The molecular structure of MB<sup>17</sup>.

treating water that has been tainted by toxic chemicals is essential for both environmental preservation and the repurposing of these unusual water<sup>13–16</sup>.

Various physical processes exist for the removal of dyes from wastewater discharges. Among the most effectively employed methods are filtration processes (membrane, nanofiltration, ultra/microfiltration), reverse osmosis, ion exchange, irradiation, electrolysis, coagulation-flocculation, and adsorption techniques<sup>18–21</sup>. Solid sorbents were utilized in adsorption technique to remove dyes like MB. The method has been used extensively and successfully to extract MB from wastewater. Numerous adsorbents have been studied and successfully used to lower the concentrations of dyes in aqueous solutions<sup>22</sup>. This organic material was removed from aquatic media using a variety of natural and synthetic adsorbents, including magnetic chitosan, zeolite, kaolin<sup>23–25</sup>, activated carbon, natural clay, Fe<sub>3</sub>O<sub>4</sub>/activated montmorillonite nanocomposite, and kaolin<sup>26–30</sup>.

Among the synthetic adsorbents, geo-polymers are mostly utilized to eliminate organic materials<sup>31</sup>. In the 1970s, Professor Joseph Davidovits introduced the word “geopolymer” to the globe. The prefix “geo” stands for inorganic aluminosilicate, which is derived from geological sources and forms geopolymer through a polycondensation reaction with an alkaline solution<sup>32</sup>. The overall configuration of the geopolymer materials is mostly determined by the Si/Al ratio in the structural chains of the polymeric building blocks, which determines the three major forms of geopolymers<sup>33,34</sup>.

The selection of raw materials for the production of geopolymer is influenced by several aspects, including affordability, accessibility, application specificity, and end users’ express interest. Every source material has benefits and drawbacks. Poly-silicate include fine silica powder made from ferro-silicon metallurgy or sodium or potassium silicate supplied by the synthetic industry. to some extent Partially Dealuminated metakaolin (PDK) is a residual material produced after the chemical leaching of MK (such as calcined kaolin or Al<sub>2</sub>O<sub>3</sub>·2SiO<sub>2</sub>) in the aluminum sulfate industry<sup>35</sup>. The SiO<sub>2</sub>/Al<sub>2</sub>O<sub>3</sub> ratio increased as a consequence of the dealumination procedure. The enhanced specific surface resulting from acid attack is attributed to the expansion of the pore volume, without a significant increase in the average pore size distribution<sup>36</sup>.

Clay is frequently used as the first ingredient to create geopolymers since it is inexpensive and readily available in large quantities<sup>37–39</sup>. Using kaolinite that has undergone pre-treatment and the resultant calcined metakaolin as the starting material for geopolymer synthesis is the subject of some noteworthy research on clay-based geopolymer<sup>40,41</sup>.

An essential role in the creation of geopolymer is played by the alkaline activator. The metal cation balances the negative charge in the framework formed by the tetrahedral aluminum, and the OH<sup>-</sup> ion can function as a catalyst in the process<sup>42</sup>. Because the Na<sup>+</sup> ion is smaller and has a larger charge density than the K<sup>+</sup> ion, it migrates across the gel network more quickly and efficiently, giving NaOH a stronger dissolving capacity than KOH<sup>43</sup>.

The analysis of PDK verified the existence of quartz and highly amorphous silica, which has a large surface area thereby suggesting a high level of reactivity. A typical consequence of acid attack on metakaolin is the breakdown of aluminum structures from octahedral and tetrahedral positions, resulting in the formation of unbound silica. Consequently, aluminum ions are being extracted from the lattice without disrupting its structure and exposing vacancies for replacement by other metal ions.

The purpose of this study is to efficiently synthesize geopolymer from partially dealuminated metakaolin (PDK) which is an industrial residue of kaolin-based aluminum sulfate manufacturing process, and to present the using of the synthesized geopolymer for removal of methylene blue from wastewater. In this work the synthesized materials were characterized using several techniques to analysis the structure and morphology of the obtained geopolymer.

This work synthesized the metakaolin-based geopolymer using a geopolymerization process. The developed adsorbent’s morphological and structural characteristics were described using FTIR, SEM, XRF, XRD, and BET analyses. Adsorbent dose, pH, contact time, and initial dye concentration, were among the several experimental settings used to examine the developed sample’s adsorption characteristics. In order to examine the batch adsorption process of the basic dye utilizing the synthesized metakaolin-based geopolymer, adsorption kinetics and isotherm data were examined (Fig. 2).

## Materials and experimental methods

### Materials

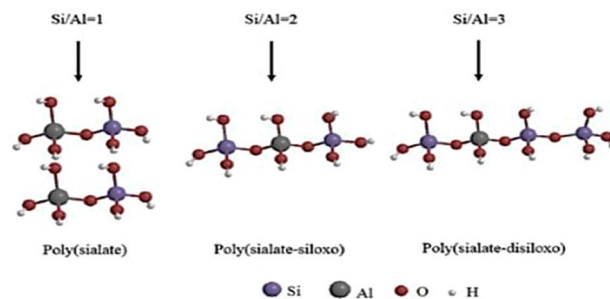


**Fig. 2.** Patterns of aluminosilicate chains<sup>44</sup>.

Chemical	Source
Partial Dealuminated Metakaolin (PDK)	Aluminum sulfate factory, Egypt
Metakaolin (MK)	Aluminum sulfate factory, Egypt
Hydrochloric Acid (HCl), Purity 99.99%	Merck, Germany
Sodium Hydroxide (NaOH) Purity 99.99%	Merck, Germany
Methylene Blue (MB) Purity 99.99%	Merck, Germany

#### Preparation of geopolymer

Figure 3 shows that the activator solution was prepared by adding of PDK powder to NaOH solution (12 M), this mixture was stirred at room temperature for period of 15 min. MK was added to the activator in a mixer at ambient temperature for 15 min with constant agitation to achieve optimal homogenization. The formed paste was mixed within ten minutes at room temperature before being poured into the cubic-plastic mold (50 × 50 × 50 mm) followed by drying at 70° C for 24 h. The formed geopolymer were ground and sieved to be between 63–200 μm, followed by washing in an excess amount of distilled water until the pH reached a neutral value. Compressive strength was measured to determine the mechanical properties of the geopolymer (Table 1).

#### Characterization

Fourier Transform Infra-Red (FTIR) spectroscopy was applied to analyse the structure of geopolymers in combination with X-ray diffraction (XRD). This is because geopolymers are amorphous material, and cannot be described using only XRD. To confirm the formation of geopolymer and characterize the interaction between PDK in the presence of alkaline activation and MK, Fourier Transform Infra-Red (FTIR) spectra were recorded in a JASCO FT-IR/4100 spectrometer. The dried samples were ground with potassium bromide (KBr) in a portion of 1/10 (wt %) and scanned in the transmittance model. Spectra were taken from 4000 to 400 cm<sup>-1</sup> wavenumber with a resolution of 2 cm<sup>-1</sup>.

The structure of PDK, and geopolymers such as the crystalline and amorphous forms was observed by XRD (Smart Lab, Rigaku, Japan) with Cu K<sub>α</sub> radiation ( $\lambda = 1.54056 \text{ \AA}$ ) at 40 kV and 30 mA. The XRD patterns were taken in the  $2\theta$  range from 10 to 40°, while the scanning speed was 0.01°/min. The surface topography and the structural composition of the samples were scanned using a Scanning Electron Microscope – Energy Dispersive X-Ray Spectroscopy. SEM (JSM-IT300, JEOL, Japan). Samples were coated with a thin layer of conducting material (gold) and imaged at various magnifications with an accelerating voltage of 10–15 kV. In addition, to observe the element distributions in the obtained geopolymers, an EDS (JSM-5300LV; JEOL Ltd., Japan) was also equipped.

M: Molar ratio.

Molar ratio = weight / molecular weight. For silica weight (g) divided by 60; For Alumina weight (g) divided by 102.

#### Adsorption experiment of MB

A stock solution of MB (1000 mg/L) was prepared by dissolving MB in deionized water at a pH of 8. The adsorbent mass of the prepared geopolymer started with a dose of 350 mg and was placed in 50 mL of MB solutions containing 10, 20, 30, 40, 50, and 60 ppm. The mixtures were stirred for 180 min at 200 rpm and 298 K. After that, the sample was filtered with glass fiber filter paper. The initial and residual concentrations were measured using a UV–Vis spectrophotometer (V-750, Jasco, Japan) at a wavelength of 662 nm for MB. The removal percentage (R, %) of the geopolymers was determined using Eq. (1), and the adsorption capacity at any time  $q_t$  (mg/g) and adsorption capacity at equilibrium  $q_e$  (mg/g) were calculated using Eq. (2).

$$R (\%) = C_o - C_t / C_o \times 100 \quad (1)$$

where R was the removal capacity of the dyes adsorbed (%), and  $C_o$  and  $C_t$  were the initial and equilibrium concentrations of dyes in the solution (mg/L), respectively.



Fig. 3. Preparation of geopolymer.

Sample	MK (g)	SiO <sub>2</sub>	Al <sub>2</sub> O <sub>3</sub>	Partially de-Aluminated metakaolin	SiO <sub>2</sub>	Al <sub>2</sub> O <sub>3</sub>	Total SiO <sub>2</sub> Total Al <sub>2</sub> O <sub>3</sub>	NaOH (g)	Water (g)	Average Compressive Strength (MPa)	Molar ratio SiO <sub>2</sub> /Al <sub>2</sub> O <sub>3</sub>
				"Source of Silica" (g)							
#1	280	116.8 1.95 M	98 0.96 M	264	167.1 2.78 M	16.4 0.16 M	4.73 1.12	140	126	21	4.2
#2	330	137.6 2.29 M	115.5 1.13 M	205	129.8 2.16 M	12.7 0.125 M	4.45 1.26	165	110	28	3.5
#3	377	157.2 2.62 M	132 1.29	151	95.6 1.59 M	9.4 0.092	4.21 1.38	188	95	43	3.05
#4	425	177.2 2.95 M	148.8 1.46 M	94	59.5 0.99 M	5.8 0.057 M	3.94 1.52	212	80	32	2.6

Table 1. Geopolymer ingredients, and the mix design.



$$q_{t,e} = (C_o - C_t) \times V/M \quad (2)$$

where  $C_o$  and  $C_t$  (mg/L) were the concentrations of the solution at the initial time and a time  $t$  (h), respectively,  $C_e$  (mg/L) was the equilibrium concentration of dye solution,  $V$  (L) was the volume of the contaminated solution, and  $M$  (g) was the weight of the dried adsorbent.

### Kinetic experiments

A Pyrex glass beaker with a volume of 2 L was used for kinetic process experiments. In the beaker, 1 L of MB aqueous solution at 50 mg/L was added and the pH was set to 7. The beaker cell's centre was fixed with a three-bladed stainless-steel axial flow impeller. At room temperature, the impeller's agitation was begun at 200 rpm. The exact weight of adsorbent was applied at zero-time interval. At various time periods, samples from the beaker were obtained. The ultimate equilibrium MB concentration of these samples was determined after they were filtered and examined. The concentration time decay curves were produced by plotting the  $C_e/C_o$  vs. time.

### Adsorption kinetics models

#### Pseudo-first-order kinetic model

This model may be expressed with reliability using the Lagergren equation. It describes how the MB adsorbed by geopolymer kinetically<sup>45</sup>. The Eq. (3) represents the model<sup>46</sup>:

$$dq/dt = k_1 (q_e - q_t) \quad (3)$$

where  $q_t$  (mg/g) and  $q_e$  (mg/g) are the solute amounts adsorbed at any given time  $t$  (min) and equilibrium, respectively. The pseudo-first order rate constant is  $k_1$  ( $\text{min}^{-1}$ ). Take integration of Eq. (3), depending on the boundary conditions of  $q_t = 0$  at  $t = 0$  and  $q_t = q_t$  at  $t = t$ , the equation becomes Eq. (4) ref.<sup>46</sup>:

$$\ln(q_e - q_t) = \ln q_e - (K_1 t) \quad (4)$$

The plotting of  $\ln(q_e - q_t)$  versus yield the slope ( $k_1$ ) and intercept ( $\ln q_e$ ). The equilibrium MB solute uptake ( $q_e$ ) and first order kinetic constant ( $k_1$ ) can eventually be determined.

#### Pseudo-second-order kinetic model

The pseudo second-order model is represented by the equation below. As illustrated below in Eq. (5), the mass transfer of driving force,  $(q_e - q_t)$ , is proportional to the number of unoccupied sites.<sup>47</sup>:

$$dq/dt = k_2 (q_e - q_t)^2 \quad (5)$$

Taking integration of Eq. (5) whilst considering boundary conditions of  $q_t = 0$  at  $t = 0$  and  $q_t = q_t$  at  $t = t$ , the equation converts to Eq. (6):

$$1/(q_e - q_t) = 1/q_e + k_2 t \quad (6)$$

where  $k_2$  is a second-order rate constant. To illustrate a linear relationship, rearrange Eq. (6) as follows in Eq. 7:

$$t/q_t = (1/k_2 q_e^2 + t/q_e) \quad (7)$$

The connection between  $t/q_t$  and  $t$  yields the slope ( $1/q_e$ ) and intercept  $1/(k_2 q_e^2)$ . Finally, the second order rate constant ( $k_2$ ) and the amount.

## Results and discussion

### Partially de-aluminate metakaolin (PDK) and Metakaolin

XRF analysis revealed a high fineness for PDK with an average diameter of  $\sim 9.5 \mu\text{m}$ , and the average diameter of MK was  $\sim 9.5 \mu\text{m}$  with an average diameter of  $\sim 4.5 \mu\text{m}$ . The chemical composition of metakaolin (MK) and partially de-aluminated metakaolin is shown in Table 2. The major constituents of PDK and MK were silica, and alumina. Therefore, they are a good source for the basic ingredients for geopolymer.

### SEM of PDK and MK

SEM investigation was performed on MK and PDK (Fig. 4a, b). Figure 4a shows that after calcination of kaolin, the obvious layered structure of kaolin had been destroyed and replaced by the disordered scale-like arrangement structure. The layered morphology of PDK is clear, and evidences increasing of the surface area that may reflect the reactivity of PDK.

### The chemical composition of geopolymer

The prepared geopolymer that achieved higher compressive strength was as listed in Table 3. According to XRF investigation  $\text{SiO}_2$ ,  $\text{Al}_2\text{O}_3$ , and  $\text{Na}_2\text{O}$  as showed in table are the primary components that are responsible for the formation of geopolymer<sup>48</sup>.

### X-Ray diffraction

The amorphous phase presence suggests that the geopolymer matrix has been effectively formed, as this chaotic structure is typically associated with geopolymers. The quartz that is observed is likely a byproduct of the

Parameter	Amount (weight %)	
	PDK	MK
SiO <sub>2</sub> (quartz)	21.2	16.3
SiO <sub>2</sub> (amorphous)	63.3	41.7
Al <sub>2</sub> O <sub>3</sub>	6.2	35
Fe <sub>2</sub> O <sub>3</sub>	0.6	1.2
TiO <sub>2</sub>	2.8	2.6
MgO	0.11	0.15
CaO	0.13	0.51
Na <sub>2</sub> O	0.07	0.13
K <sub>2</sub> O	0.05	0.07
SO <sub>3</sub>	1.2	0.55
Cl <sup>-</sup>	0.06	0.11
LOI	3.56	1.0
Total	99.28	99.32

**Table 2.** The chemical composition of PDK, and MK.

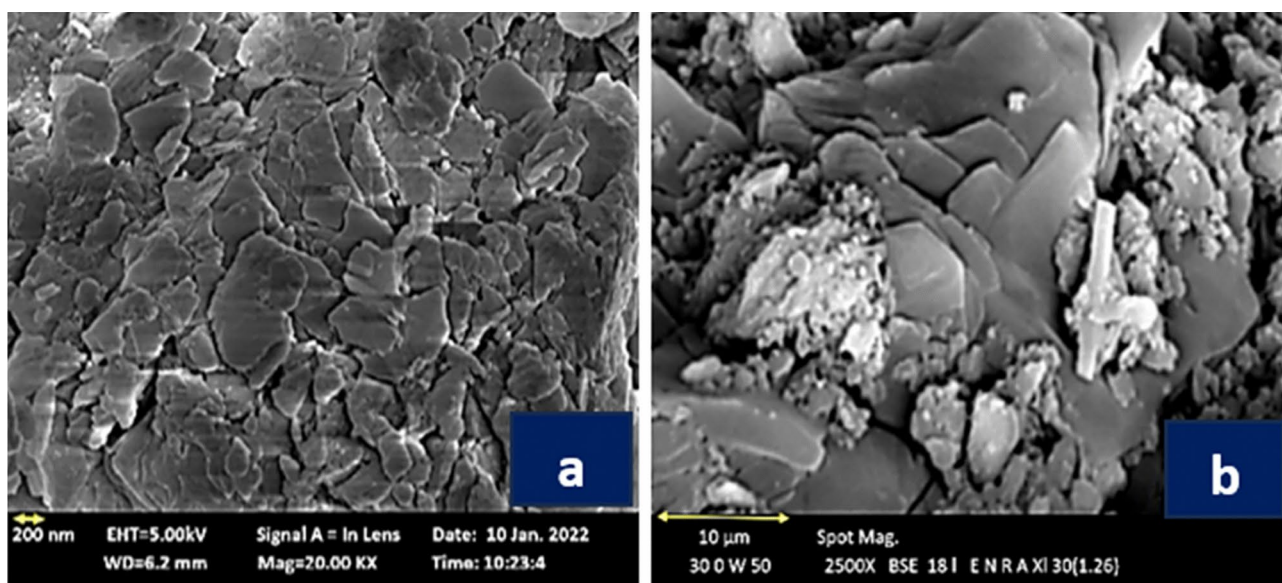


**Fig. 4.** SEM of MK (a) and PDK (b).

The parameters (%)									
SiO <sub>2</sub>	Al <sub>2</sub> O <sub>3</sub>	Fe <sub>2</sub> O <sub>3</sub>	TiO <sub>2</sub>	Na <sub>2</sub> O	CaO	P <sub>2</sub> O <sub>5</sub>	Cl	Loss of Ignition	Total
55.7	20.7	1.44	2.14	7.6	0.32	0.09	0.03	16.3	99.33

**Table 3.** XRF of the highest compressive strength prepared geopolymer.

metakaolin or other additives, and it does not endure a complete reaction during the geopolymerization process. In these systems, quartz frequently demonstrates inertness<sup>49,50</sup>. The anatase phase's existence may be attributed to the incorporation of TiO<sub>2</sub> in the primary materials or as an addition. In the geopolymer, the X-ray diffraction (XRD) pattern indicates the presence of unreacted crystalline phases, including anatase and quartz, as well as an amorphous geopolymer matrix (characterized by a large ridge). The material possesses a predominantly amorphous structure, which is typically found in geopolymers. Nevertheless, the geopolymer's unreacted substances or additives are illuminated by the presence of crystalline components, as indicated in Fig. 4 ref.<sup>51,52</sup>.

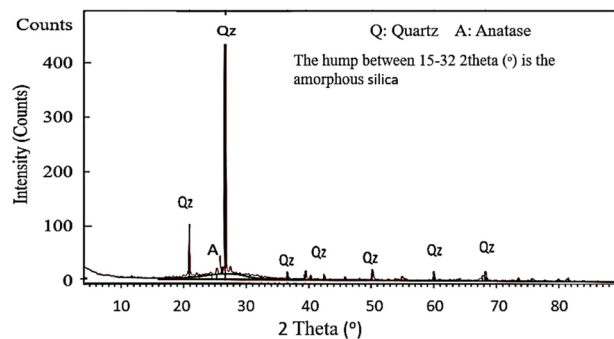


**Fig. 5.** XRD of geopolymer of highest compressive strength.

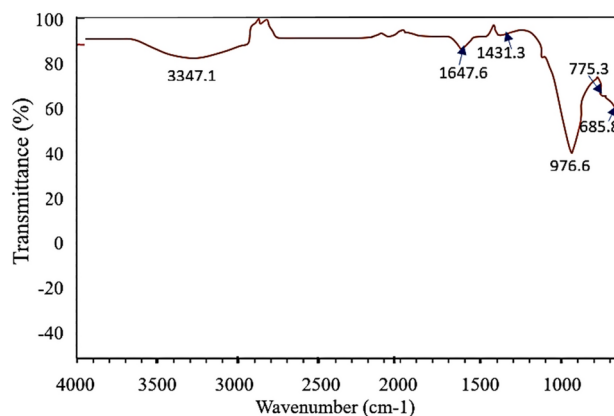


**Fig. 6.** FTIR spectrum of the prepared geopolymer.

### FTIR spectra

The spectral pattern of the geopolymer (Fig. 5) exhibits a broad band between 3000 and 3600  $\text{cm}^{-1}$ , and another weak one located at 1647.6  $\text{cm}^{-1}$ , which are attributed respectively to the low-energy O–H bond and the H–O–H functional group, resulting from free water molecules, either sorbed on the surface or caught between the recesses of the geopolymeric framework<sup>53,54</sup>. The sharp absorption band appearing at 1430  $\text{cm}^{-1}$  in the geopolymer product is related to the vibrational stretching of the O–C–O bond, due to the presence of carbonate<sup>55</sup>. The appearance of later band refers to the unreacted NaOH, which was combined with carbon dioxide from the surrounding medium<sup>56</sup>. Then, the band at 976.6  $\text{cm}^{-1}$  corresponding to stretching vibration of Si–O–T (T = Si or Al). This change can be interpreted by the occurrence of a geopolymerization reaction that included the dissolution process and the condensation reaction forming new bonds, which form oligomers  $[\text{Si–O–Al–O–Na}]$ - which polymerized, forming the sodium aluminum silicate hydrate gel [N–A–S–H gel]<sup>57</sup>.

It was also noted that the band positioned at 685.8  $\text{cm}^{-1}$  assigned to stretching vibrations of the Si–O quartz<sup>58,59</sup>. These findings are in agreement with the XRD results observed above.

Figure 6 illustrates the Image of surface morphology of a geopolymer particle at 500 $\times$  magnification. The surface is rough and granular, like metakaolin-based geopolymers. For adsorption, roughness improves surface area for pollutant interaction like methylene blue. The selected location appears to have irregularly shaped particles or clusters. Geopolymer networks, generated by polycondensation of aluminosilicate materials (metakaolin) in an alkaline media, have this irregularity. Small particles or agglomerates on the surface indicate a heterogeneous geopolymerization structure. These tiny particles may be unreacted metakaolin or other geopolymerization phases<sup>60</sup>. EDX microanalysis analysed the elemental composition of metakaolin and geopolymer. EDX analysis showed that oxygen, sodium, aluminium, and silicon made up 49, 10.6, 11, and 26% respectively of the mixture. The composition of the geopolymer complies with XRF<sup>61</sup>.

the EDS mapping showed that the distribution of the elements in the prepared geopolymer was significantly different from the Si content due to the increased loading amount of PDK during the geopolymerization.

### Batch adsorption testing

The pH is an important parameter in determining the effect of the aqueous medium on the adsorption capacity of a material. It was known that high concentrations of  $\text{H}^+$  ions were at low pH (below 7). Hence, these  $\text{H}^+$  ions compete with MB cations on the binding sites of adsorbing material. As a result, electrostatic repulsion takes place, reducing the adsorption capacity of MB on the surface of the geopolymer. On the other size, at higher pH, a negatively charged surface of the geopolymer is formed from the predominance of  $\text{OH}^-$  ions in the solution.

Initial concentration $C_0$ (mg/L)	Removal capacity (%)	Uptake amount $Q_e$ (mg/g)
10	100	1.42
20	99.5	2.8
30	99	4.2
40	95	5.4
50	94	6.7
60	92	8

**Table 4.** Value of the Removal Capacity (%) and Uptake Amount (mg/g) of MB Adsorption of the Obtained Geopolymer at pH 8.

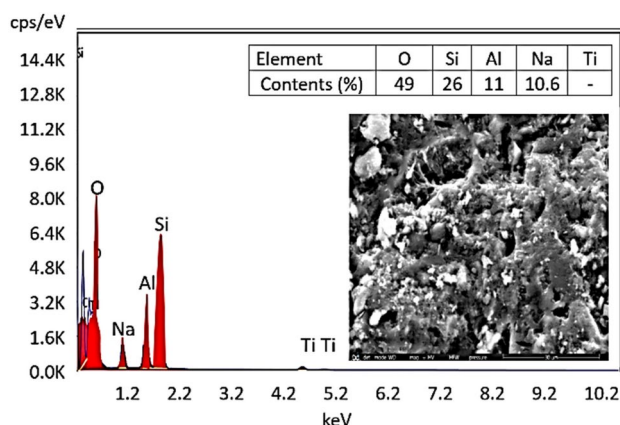


**Fig. 7.** SEM – EDS mapping of the prepared geopolymer.

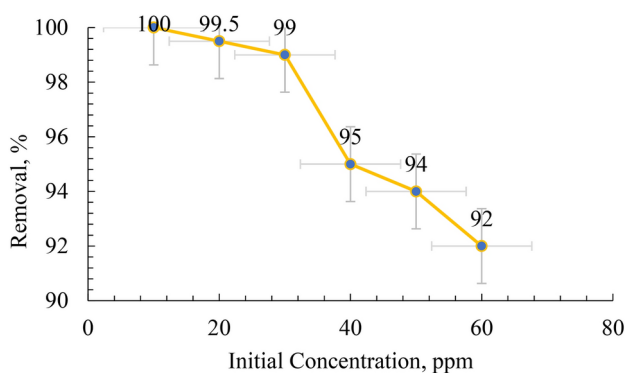


**Fig. 8.** Removal percentage at different initial concentrations of MB.

Therefore, an increase in the adsorption capacity of the geopolymers for MB ions is achieved, based on the electrostatic attraction. In this work, pH 8 was selected because this value is close to neutral, which does not need pH adjustment in the applications.

#### Effect of initial concentration of MB on its removal

The effect of initial concentration of MB on its removal by the geopolymer powders is shown in Table 4, and Figs. 7, 8 and 9. The graph shows the impact of the starting concentration of methylene blue on the effectiveness of its removal by a geopolymer of metakaolin-based composition. Once the initial concentration of MB rises from 10 to 60 ppm, there is a progressive decline in the effectiveness of removal. More precisely, the percentage of elimination decreases from just over 100% at lower concentrations (10 ppm) to 92% at the maximum dosage (60 ppm).

This phenomenon is frequently observed in adsorption processes, where the starting concentration of the pollutant greatly influences the adsorption capacity of the adsorbent, namely the geopolymer in this instance. At reduced concentrations of MB, the abundance of adsorption sites on the geopolymer surface is adequate





**Fig. 9.** Removal of MB with different concentration by the prepared geopolymer.

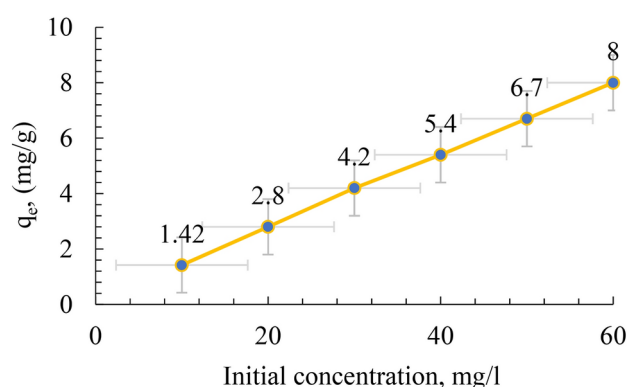


**Fig. 10.** Effect of initial MB dye concentration on the adsorption capacity.

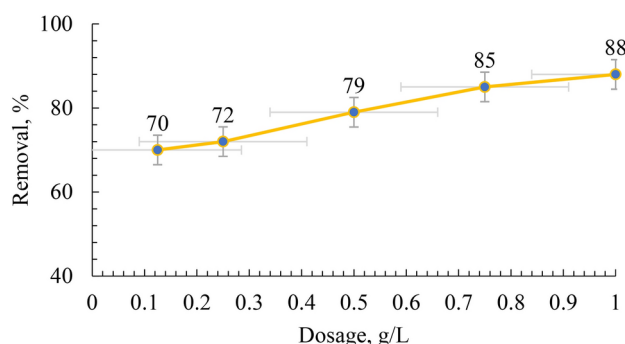


**Fig. 11.** Effect of GP dose on the removal of MB at pH 7 for 60 min.

to capture almost all the dye molecules, leading to almost total elimination. Table 4 shows that the adsorption capacity increases as the initial concentration increases.

#### Effect of geopolymer dose on MB removal

The removal of MB was examined in relation to the adsorbent dose, and the results are illustrated in Fig. 10. It is evident that when the geopolymer dose increase from 0.1 to 1 g/L, the elimination of MB increased from 70 to 88% at pH 7. These results may be attributed to the growing number of bindings sites in the geopolymer, which increases the number of adsorbents and enhances the removal of MB. Controlling the adsorption capacity greatly depends on optimizing the capacity of the adsorbent. Increasing the quantity of adsorbents may result in more binding sites in the geopolymer for MB removal. Optimizing adsorbent mass is crucial for controlling adsorption capacity.

Figure 11 presents the adsorption capacity of MB as a function of adsorbent dosage at a fixed MB concentration ( $60 \text{ mg L}^{-1}$ ) and volume (50 mL). The results reveal that the adsorption capacity obtained for 0.125 to 1.0 g dosage ranged from 6.36 to 8.0 mg.  $\text{g}^{-1}$ . The overall, an upsurge in the removal and adsorption

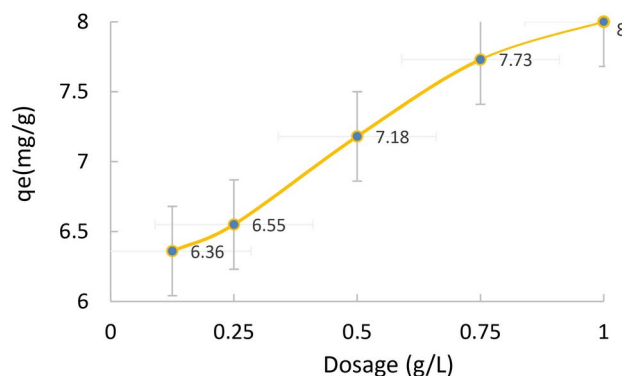


**Fig. 12.** Effect of GP dose on the adsorption capacity of MB at pH 7 for 60 min.

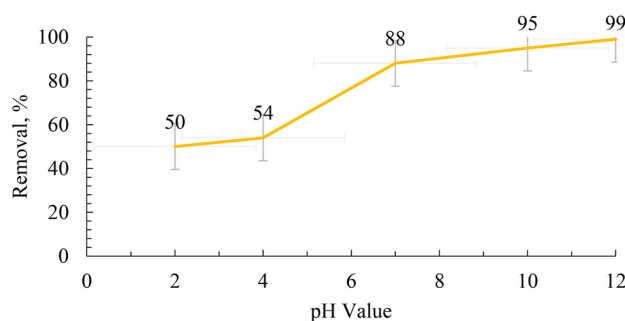


**Fig. 13.** Effects of pH on the MB adsorption by GP initial Methylene Blue (MB) concentration = 60 ppm, GP 0.35 g and temperature = 25 °C for 60 min.

capacity is attained with the increase in adsorbent dosage, and the trend is explained as with more adsorbent, there is an increase in adsorption sites due to the presence of more adsorbent materials. The adsorption capacity increases with the higher adsorbent doses due to increased surface area, active sites availability, and interaction possibilities. This enhances the efficiency and leads to multilayer adsorption<sup>62</sup>.

### Effect of pH on removal

The pH level significantly affects the elimination of organic materials from water. Figure 12 illustrates the impact of the initial pH of the solution on the adsorption process. It has been shown that the effectiveness of removal rises as the pH value increases, reaching 98.4% at a pH value of 12. The elimination process is influenced by the alteration in the pH level of the solution. When the geopolymer is in an acidic environment, the surface of the material is enveloped by  $H^+$  ions. This leads to a reduction in the interaction between the solute ions ( $MB^+$ ) and the sites on the geopolymeric material. In contrast, in the neutral solution, the concentration of  $H^+$  ions reduce, leading to a favorable interaction between the dye ions and the surface sites. The increase in removal can be attributed to the electrostatic interaction between the negatively charged particles of the geopolymer and the positively charged cationic dye. The findings indicate that the interaction between the inorganic framework (with a negative charge) and methylene blue (with a positive charge) is pH-dependent.

### Effect of contact time

The impact of contact time on the removal of MB by the geopolymer is illustrated in Fig. 13. The results indicate that the removal percentage of MB is initially rapid within the first 60 min of contact time. Subsequently, equilibrium is achieved within 180 min. After reaching equilibrium, there is no significant change in the removal percentage of the geopolymer across different dye concentrations.

The results indicated that the prepared geopolymer from PDK has achieved good performance and it can be compared with other adsorbents for removal of MB as illustrated in Table 5.

### Adsorption isotherm

For studying the adsorption process, it is an important issue to investigate the equilibrium of adsorption which is normally named adsorption isotherm. The adsorption of MB dye can be upgraded by determination the equilibrium curve correlation. The isotherms of adsorption describe the equilibrium state between MB dye that is adsorbed by the sites of the GP and the MB dye amount in solution. There are number of isotherm models that describe the adsorption were adopted such as Freundlich (1907), Langmuir (1918), Redlich and Peterson

Adsorbent Type	MB conc	Adsorbent dose	pH	Contact time	Adsorption capacity	References
-Fly ash geopolymers monoliths	1 – 50 mg/L	0.11–0.55 g	2–12	30 h	15.4 mg/g	<sup>63</sup>
-Fly Ash –based geopolymers spheres	(10 – 250) mg/L	(1–2.5) g/ 0.2 L	–	24 h	30.1 mg/g	<sup>64</sup>
-Clay and rice husk geopolymer	25 mg/L	0.1 g	3	20–80 min	15.95, 14.9, and 20.2 mg/g	<sup>65</sup>
-Red mud and rice husk based geopolymer composite	(20– 120) mg/L	0.1 g	8	180 min	6.59 – 10.74 mg/g	<sup>66</sup>
-Partially dealuminated metakaolin and Metakaolin	(10–60) mg	0.35	7	60 min	8 mg/g	This study

**Table 5.** The adsorption capacity of MB dye and the influence of geopolymer developed from different industrial wastes previous works and in this study.

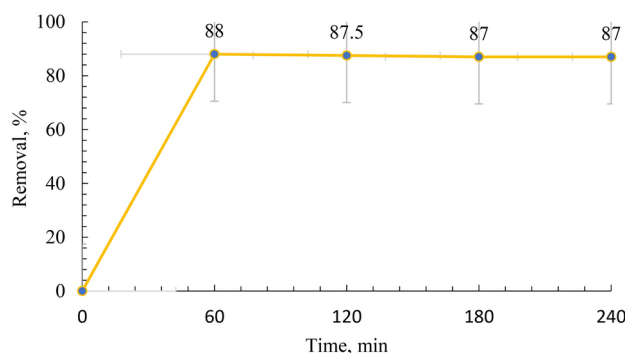


**Fig. 14.** Effects of contact time on the Mb adsorbing by GP (pH=7, initial Methylene Blue (MB) concentration = 60 ppm, GP 0.35 g and temperature = 25 °C.

(1959), Temkin, Dubinin Radushkevich. Freundlich, Langmuir are the most applied models for describing how the adsorption takes place<sup>67</sup>.

In this work, the adsorption results were assessed with the common models; Langmuir, Freundlich, and Temkin, to clarify the relationship between the adsorbent geopolymer and the MB dye in the solution.

**Langmuir isothermal model** describe of the monolayer adsorption and the homogeneity of surface sites<sup>42</sup>. For the adsorption occurring without reactions between the adsorbent species, the straight-line relationship of Langmuir was calculated by the following Eq. (8):

$$C_e/q_e = q/K_L q_m + C_e/q_m \quad (8)$$

whereas  $C_e$  is the concentration of MB dye in the solution at the equilibrium (mg/L),  $q_e$  is the capacity of adsorption per unit mass at the equilibrium (mg/g),  $q_m$  is the maximum adsorbate per unit mass of adsorbent after complete coverage of one layer on geopolymer (mg/g), and  $K_L$  is the Langmuir constant (L/mg). Plotting  $C_e/q_e$  versus  $C_e$  by using geopolymer is shown in Fig. 14a. The obtained data shows that the linear regression coefficient  $R^2$  value = 0.886 for the model of Langmuir<sup>23,68–70</sup>. The dimensionless constant or the equilibrium parameters ( $R_L$ ) is one of the most important parameters of the Langmuir model, which reflects the nature of the adsorption process.  $R_L$  value is calculated from Eq. (9) ref.<sup>37,38</sup>.

$$R_L = 1/(1 + R_L C_0) \quad (9)$$

Where  $R_L$  is the Langmuir constant and  $C_0$  is the initial concentration of MB dye. The calculated  $R_L$  value of MB dye is between zero and one ( $0 < R_L < 1$ ). Such a result illustrates that the absorbability of MB is favorable by using geopolymer.

The isotherms of MB dye adsorption on geopolymer are illustrated in Figs. 14a, b and c, and the regression coefficient are depicted in the related figures.

**Freundlich isothermal model** suppose that the sites of adsorption are heterogeneous and the adsorbing materials take up the strong available binding sites quickly. The linear regression relationship can be represented by the logarithmic Eq. (10):

$$\log q_e = (1/n) \log C_e + \log K_F \quad (10)$$

whereas  $K_F$  is Freundlich model constant which expresses the capacity of adsorption and  $n$  is the heterogeneity factor that predicts the occurrence of adsorption, whereas if  $n$  is greater than 1, the adsorption proceeds properly and effectively. The values of  $K_F$  and  $n$  can be determined from the linear relationship plot of  $\log q_e$  versus  $\log C_e$ , taking the intercept and the slope of the line. The  $1/n$  value obtained from the Freundlich isotherm plot is 0.68 which falls between 0 and 1 indicating the adsorption is linear and uniform throughout the surface. According to the  $1/n$  value ( $0 < 1/n < 1$ ), this isotherm is a favourable physical process Fig. 14b).

Figures 14a, b, and c display the correlation factor ( $R^2$ ) conforming to the models Freundlich, Langmuir, and Temkin. The results confirm that Freundlich isotherm model was evaluated to be better, which has a higher coefficient  $R^2$  value (0.996), while the Langmuir model was 0.886, and Temkin was 0.93. Comparing these data with that of Langmuir, it can be concluded that the Langmuir model has the lowest probability, whereas the  $R^2$  value is the lowest of all models.

**Temkin isotherm** considers the reactions between adsorbate and adsorbent. The linear equation can be calculated from Eq. (11).

$$q_e = R_T/b_T \cdot \ln C_e + R_T/b_T \ln K_T \quad (11)$$

whereas  $K_T$  is the Temkin isotherm constant ( $\text{L} \cdot \text{g}^{-1}$ ),  $b_T$  is a constant of heat of adsorption,  $R$  is the constant of universal gas ( $8.314 \text{ J} \cdot \text{mol}^{-1} \cdot \text{K}^{-1}$ ) and  $T$  is the temperature in Kelvin (K). The calculated maximum adsorption capacity ( $q_{\text{max}}$ , Cal) by using geopolymer is 8 mg/g for the adsorption rate of MB dye.

Table 6 summarizes all the parameters and their respective determination coefficients. Based on the values of the coefficient  $R^2$  (0.996) of the linear regression, the equilibrium data fit the model of Freundlich, rather than Langmuir or Temkin. For forecasting the adsorbability occurring in multilayers and for determining the adsorption capacity, the Freundlich model (Fig. 14b) was used herein<sup>24,25</sup>. The value of  $n$  greater than unity indicates a favourable adsorption taking place, this indicated that the adsorption occurs under a multilayer and heterogeneous surface for MB.

### Adsorption kinetics

The adsorption kinetics was assessed by conducting several experiments with different time periods. 0.35 mg of geopolymer was contacted with 50 mL of MB dye solution containing 60 mg/L of the dye, the mixture was stirred for different contact periods from 20 to 60 min at the ambient temperature. Figure 13 displayed that the adsorption of the MB dye by geopolymer proceeds fast through the first 60 min of the trial and continued slowly through the period from 60 to 240 min until the adsorption attained an equilibrium state within 240 min. These results are in agreement with those obtained by several researchers<sup>39,40</sup>. In the beginning the MB dye species adsorbed on the available sites for adsorption of the GP. This is rapid adsorption step due to the most active sites of the GP are free of MB. After occupation of the most active sites, the attraction force between the MB molecules with the GP gradually lowered and the rate of adsorption decreased. After filling the outer sites of the GP, the process goes through the GP taking a relatively longer time<sup>42</sup>.

The adsorption kinetics of MB onto GP was investigated using pseudo first order, pseudo second order models as shown in (Fig. 15a and b respectively, using the experimental data at various initial concentrations. The calculated parameters values obtained from the application of the two models are indicated in Table 7. By comparing  $R^2$  for each applied model and the compatibility between the estimated and observed  $q_e$  values, the most favourable model may be identified. The pseudo 2nd order  $R^2$  (0.9795) value are greater than other model (0.7812), and the  $q_e$  cal values for MB are considerably closer to the  $q_e$  experiment for MB than other kinetic models.

The connection between  $t/q_t$  and  $t$  (Fig. 15 b) yields the slope ( $1/q_e$ ) and intercept  $1/(k_2 q_e^2)$ . Finally, the second order rate constant ( $k_2$ ) and the amount of adsorbed dye per mass of composite at the final equilibrium point ( $q_e$ ) were determined (Fig. 16).

### Conclusions

This study successfully synthesized a geopolymer from partially dealuminated metakaolin (PDK) as a novel solid adsorbent for the effective removal of methylene blue (MB) from wastewater. The geopolymer was prepared using NaOH(12M) solution and PDK as alkaline activator. The geopolymer specific surface area was  $9.3 \text{ m}^2/\text{g}$ , which offered enough sites for the mass transfer and adsorption processes. At the optimal conditions of  $25^\circ\text{C}$  temperature, 60 mg/L initial concentration, at pH 7, and 240-min contact time, the geopolymer adsorbent particles demonstrated high adsorption efficiency for MB dye removal, with a maximum adsorption capacity reaching 8 mg/g with a removal efficiency of 99%. The Kinetic studies revealed that the adsorption process follows the pseudo-second-order model, indicating a chemisorption mechanism. The equilibrium data fit the Freundlich isotherm model, suggesting the adsorption occurs on a heterogeneous surface with a multilayer process. The research highlights the potential of PDK-based geopolymer as a cost-effective and environmentally friendly adsorbent for wastewater treatment, offering a sustainable approach to managing industrial by-products and addressing water pollution.

Model	Parameter	MB
Langmuir	$q_m(\text{mg/g})$	8.0
	$K_L (\text{L/mg})$	0.1
	$R^2$	0.886
Freundlich	$n$	1.47
	$R^2$	0.996
Temkin	$R^2$	0.93
	$K_T$	1.43

**Table 6.** Isotherm models parameters for Methylene blue.

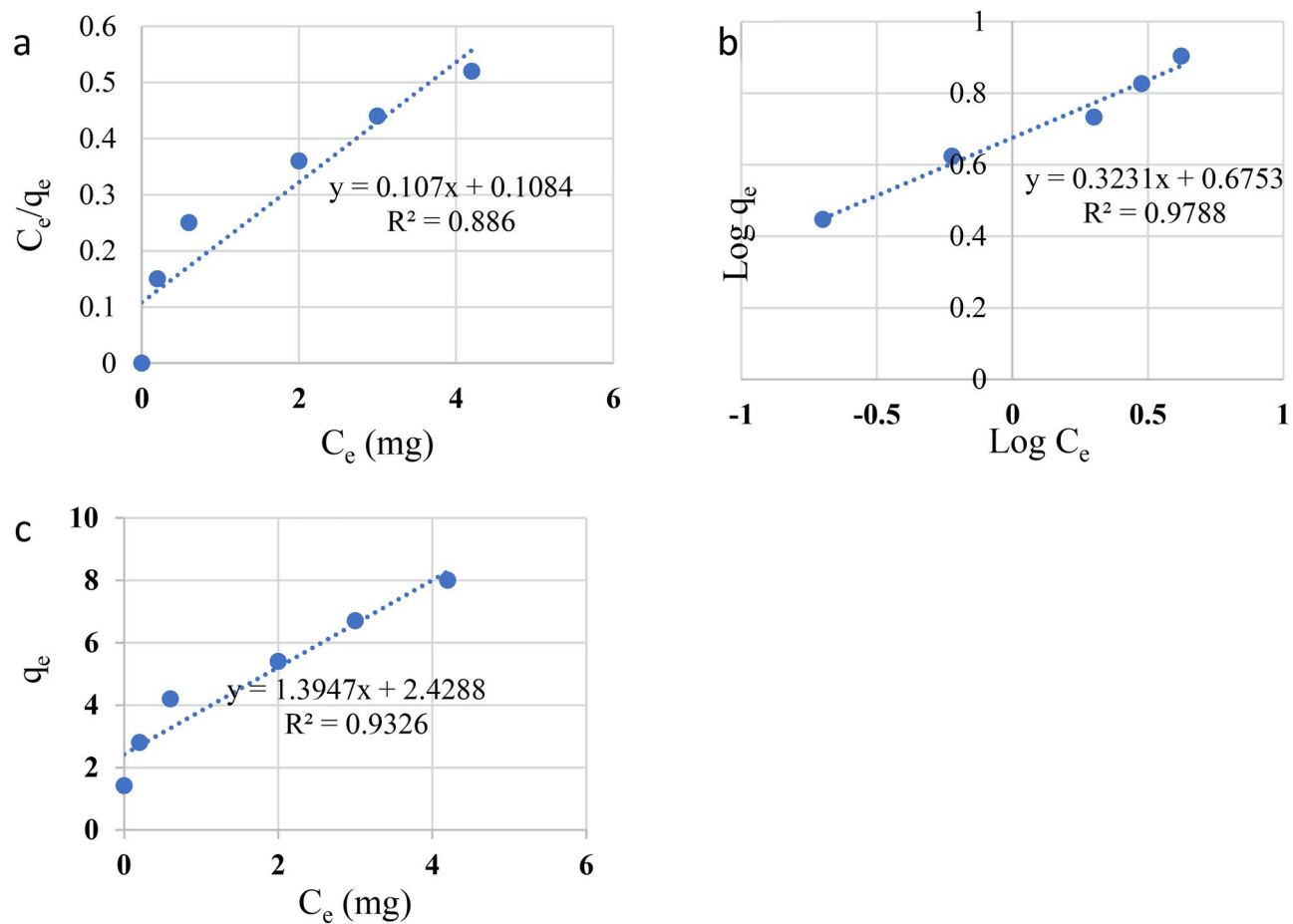


**Fig. 15.** The linear forms of adsorption isotherms fitted the equilibrium states: (a) for Langmuir (b) for Freundlich and (c) for Temkin.

Model	Parameter	MB
Pseudo-first order	$K_t$ (1/min)	-0.215
	$R^2$	0.7812
Pseudo-second order	$q_e$ (mg/g)	9.345
	$R^2$	0.9795

**Table 7.** Kinetic models parameters for Methylene blue.



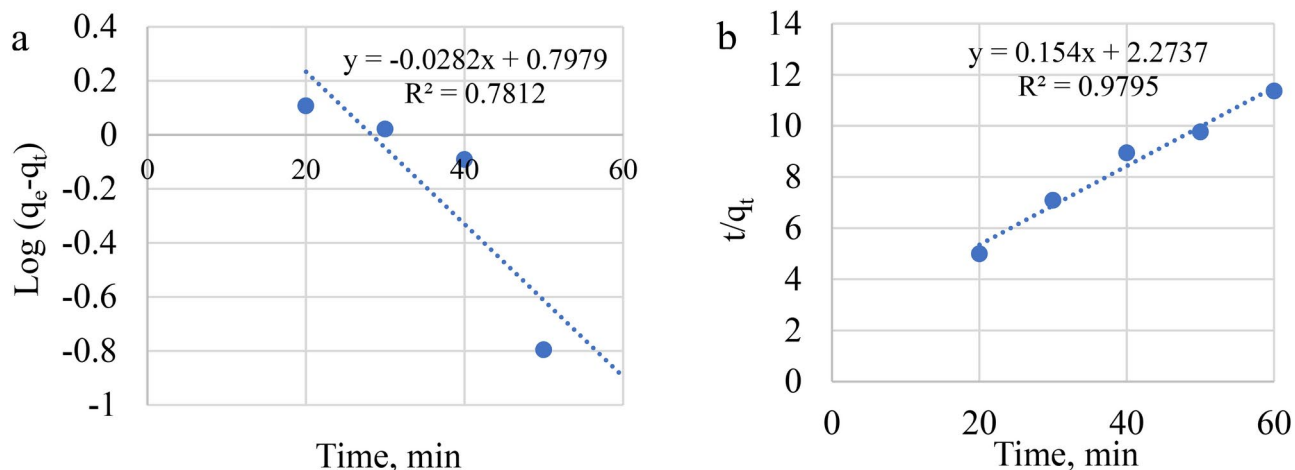


**Fig. 16.** The relation between adsorption capacity and contact time. (a) for pseudo first order, and (b) for pseudo second order.

### Data availability

All data generated or analysed during this study are included in this published article.

Received: 27 December 2024; Accepted: 6 May 2025

Published online: 21 May 2025

### References

- Pang, J. et al. Adsorption behaviors of methylene blue from aqueous solution on mesoporous birnessite. *J. Taiwan Inst. Chem. Eng.* **77**, 168–176 (2017).
- Rezaei, M. & Salem, S. Photocatalytic activity enhancement of anatase-graphene nanocomposite for methylene removal: degradation and kinetics. *Spectrochimica Acta Part A: Mo-lecular Biomol. Spectr.* **167**, 41–49 (2016).
- Jagaba AH, Kutty SRM, Fauzi MAHM, Razali MA, Hafiz MFUM, Noor A. Organic and nutrient removal from pulp and paper industry wastewater by extended aeration activated sludge system. *IOP Conf. Ser.: Earth Environ. Sci.* **842** (1):012021. (2021).
- Elewa, K., Belal, A., El Monayeri, O. & Tawfic, A. F. Application of metal-organic framework (Zn-Ph-D CP) for copper ion removal from aqueous solution. *Ain Shams Eng. J.* <https://doi.org/10.1016/j.asej.2021.101670> (2022).
- Tara, N.; Siddiqui, S.I.; Rath, G.; Chaudhry, S.A.; Inamuddin; Asiri, A.M. Nano-engineered Adsorbent for the Removal of Dyes from Water: A Review. *Curr. Anal. Chem.* **16**, 14. (2019).
- Mahdy, M.M., Mahfouz, S.Y., Tawfic, A.F., Ali, M.A.E.M. "Performance of Rice Straw Fibers on Hardened Concrete Properties under Effect of Impact Load and Gamma Radiation" *Fibers*, **11**(5), 42, <https://doi.org/10.3390/fib11050042>. (2023).
- Ahmed F. Tawfik Ahmad A. Baraka Mohammad M. Gobara Ahmed M. Omar Potential use of aqueous solution of Tartarazine dye as Low-dose dosimeter for gamma radiation, <https://doi.org/10.21608/iccee.2010.37357>, (2010).
- Khan, I., Khan, I., Usman, M., Imran, M. & Saeed, K. Nano clay-mediated photocatalytic activity enhancement of copper oxide nanoparticles for enhanced methyl orange photodegradation. *J. Mater. Sci. Mater. Electron.* **31**, 8971–8985 (2020).
- A. Abdel-Latif M, Aliaa M Monazie, Ahmed M. Al Kaisy, A.F. Tawfic, Samah A. Al- Sholkamy "Shielding and dosimetry parameters for aluminum carbon steel" *Applied Radiation and Isotopes*, 2023, <https://doi.org/10.1016/j.apradiso.2023.111022>. (2023).
- Mostafa Ahmed Abdel-Baky, EL-Desoki Ibrahim Eaid, Ibrahim Ahmed El-Khaldy, A Farghal Tawfic Investigation of natural ventilation using a solar chimney in various solar cases *International Journal of innovative research and scientific studies*, <https://doi.org/10.53894/ijirss.v7i2.2699>, (2024).
- A.F. Tawfic, S.A. Dickson, Y. Kim, W. Mekky, Enhanced Capacity and Stability for the Separation of Cesium in Electrically Switched Ion Exchange Fusion Sci. Technol. <https://doi.org/10.13182/FST14-T91>, (2015).
- Alencar, L. V. T. D., Passos, L. M. S., Soares, C. M. F., Lima, A. S. & Souza, R. L. Efficiency Method for Methylene Blue Recovery Using Aqueous Two-Phase Systems Based on Cholinium-Ionic Liquids. *J. Fash. Technol. Text. Eng.* **6**, 13–20 (2020).
- Ahmad, A. et al. Recent advances in new generation dye removal technologies: Novel search for approaches to reprocess wastewater. *RSC Adv.* **5**, 30801–30818 (2015).
- A. F. Tawfic, S. E. Dickson, Y. Kim, W. Mekky, Mohamed Gobara & Ahmad Baraka "Preparation and characterization of nickel hexacyanoferrate films for the removal of cesium ion by electrically switched ion exchange (ESIX)" *Journal of Solid State Electrochemistry*, <https://doi.org/10.1007/s10008-017-3635-y>. (2017).
- El-Afandy A, Mohamed G. El-Feky, Samia H. Taha, S. M. El Minyawi, H. A. Sallam, A. F. Tawfic, A. Omar and M. G. El-Samrah "Radioactivity and Environmental Impacts of Granites from Um Ara, Southeastern Desert, Egypt" 2023, <https://doi.org/10.1088/1742-6596/2305/1/012033>. (2023).
- Sayed, M. S. M., El-Mongy, S. A., Tawfic, A. F. & Abdel-Rahman, M. A. E. "Validation of the Optimized Parameters for Improvement of Gamma Spectrometers Performance and Efficacy. *Phys. Elementary Particles Atomic Nuclei Exp.* <https://doi.org/10.1134/S1547477121020175> (2021).
- Davidovits, J. Geopolymer chemistry and applications, (5th ed.) J. Davidovits. Geopolymer Institute. (2020).
- Ahmad, M. et al. Phytogenic fabrication of ZnO and gold decorated ZnO nanoparticles for photocatalytic degradation of Rhodamine B. *J. Environ. Chem. Eng.* **9**, 104725 (2021).
- Amin, A.M., Mahfouz, S.Y., Tawfic, A.F., Ali, M.A.E.M "Experimental investigation on static/dynamic response and  $\gamma/n$  shielding of different sustainable concrete mixtures" *Alexandria Engineering Journal*, **75**, pp. 465–477, <https://doi.org/10.1016/j.aej.2023.06.010>. (2023).
- El-Samrah, M. G., Tawfic, A. F., Sallam, F. H. & Omar, A. M. Investigation of specially designed bentonite samples as potential bricks with better radiation shielding properties. *Progress Nucl. Energy* <https://doi.org/10.1016/j.pnucene.2023.104778> (2023).

21. Pandey, S., Do, J. Y., Kim, J. & Kang, M. Fast and highly efficient removal of dye from aqueous solution using natural locust bean gum-based hydrogels as adsorbent. *Int. J. Biol. Macromol.* **143**, 60–75 (2020).
22. Shi, B., Li, G., Wang, D., Feng, C. & Tang, H. Removal of direct dyes by coagulation: the performance of preformed polymeric aluminum species. *J. Hazardous Materials* **143**(1–2), 567–574 (2007).
23. Hu, J., Dai, W. & Yan, X. Comparison study on the ad-sorption performance of methylene blue and congo red on Cu-BTC. *Desalin. Water Treat.* **57**(9), 4081–4089 (2016).
24. MS Elfawal, NH El-Ashkar, Nabil M. Nagy, Shalan, Ali H “Utilization of electric arc furnace slag and metakaolin as precursors in alkali-activated paste: microstructure and mechanical properties” *Innovative Infrastructure Solutions* **9**, 343 (2024).
25. MS Elfawal, NH El-Ashkar, NM Nagy, AH Shalan “Microstructural and mechanical characteristics of alkali-activated green concrete using slag from electric arc furnaces as precursor and aggregate” *IOP Conference Series: Earth and Environmental Science* **1396**(1). <https://doi.org/10.1088/1755-1315/1396/1/012002> (2024).
26. S. Dutta, A. Bhattacharyya, A. Ganguly, S. Gupta, S. Basu, Application of response surface methodology for preparation of low-cost adsorbent from citrus fruit peel and for removal of methylene blue, *Desalination*, **275** (1–3), 26–36. (2011).
27. Mondal, S. Methods of dye removal from dye house effluent—an overview *Environ. Eng. Sci.* **25**(3), 383–396 (2008).
28. Stephenson, R. J. & Sheldon, J. B. Coagulation and precipitation of a mechanical pulping effluent: 1. *Removal Carbon Turbidity Water Res.* **30**, 781–792 (1996).
29. G.M. Walker, L.R. Weatherley - Fixed bed adsorption of acid dyes onto activated carbon *Environ. Pollut.*, **99**, pp. 133–136. (1998).
30. Rida, K., Bouraoui, S. & Hadnine, S. Adsorption of methylene blue from aqueous solution by kaolin and zeolite. *Appl. Clay Sci.* **83–84**, 99–105 (2013).
31. Gupta, V. K. et al. Equilibrium and thermodynamic studies on the adsorption of the dye rhodamine-B onto mustard cake and activated carbon. *J. Chem. Eng. Data* **55**(11), 5225–5229 (2010).
32. Deng, H., Yang, L., Tao, G. & Dai, J. Preparation and characterization of activated carbon from cotton stalk by microwave assisted chemical activation-application in methylene blue adsorption from aqueous solution. *Journal of Hazardous Materials* **166**(2–3), 1514–1521 (2009).
33. Bentahar, S., Dbik, A., Khomri, M. E., Messaoudi, N. E. & Lacherai, A. Adsorption of methylene blue, crystal violet and congo red from binary and ternary systems with natural clay: kinetic, isotherm, and thermodynamic. *J. Environ-Mental Chem. Eng.* **5**, 5921–5932 (2017).
34. Liang, K., Wang, X. Q., Chow, C. L. & Lau, D. A review of geopolymer and its adsorption capacity with molecular insights: A promising adsorbent of heavy metal ions. *J. Environ. Manage.* **322**, 116066 (2022).
35. Ahmed, E. S. A. et al. Synthesis of Faujasite-Na-type zeolite from partial de-aluminated metakaolin for removal of methylene blue from contaminated water. *Chem. Pap.* <https://doi.org/10.1007/s11696-025-03950-8> (2025).
36. Nabil A. Al-Sagheer, Gamal Aboulfotouh, Noura F. Abdel Salam, Fayza S. Hashem. Extraction of silicon oxide from the partially dealuminated metakaolin residue of the kaolin-based aluminum sulfate manufacturing process. *Egyptian Journal of Petroleum* **33**, 567–576. <https://doi.org/10.62593/2090-2468.1051>. (2024).
37. Ibrahim, W. et al. *Technological Properties of Fly Ash-Based Lightweight Geopolymer Brick* (Springer, London, 2021).
38. Abdullah, Nabil & El-sokkary, T.M. & Gharieb, Mahmoud. Synthesis of geopolymer binder from the partially de-aluminated Metakaolinite by-product resulted from alum industry. **74**, 166, (2023).
39. Tahmasebi Yamchelou, M., Law, D., Brkljača, R., Gunasekara, C., Li, J., & Patnaikuni, I. Geopolymer synthesis using low-grade clays. *Construction and Building Materials* **2**, 268 (2021).
40. Pourabbas Bilondi, M., Toufigh, M. M. & Toufigh, V. Experimental investigation of using a recycled glass powder-based geopolymer to improve the mechanical behaviour of clay soils. *Constr. Build. Mater.* **170**, 302–313 (2018).
41. Zhang, Y. et al. Effect of particle size and curing temperature on mechanical and microstructural properties of waste glass-slag-based and waste glass-fly ash-based geopolymers. *J. Clean. Prod.* **273**, 122970 (2020).
42. Ren, B., Zhao, Y., Bai, H., Kang, S., Zhang, T., & Song, S. Eco-friendly geopolymer prepared from solid wastes: A critical review. *Chemosphere.* (2021).
43. Lemougna, P. N., Wang, K., Tang, Q., Melo, U. C. & Cui, X. Recent developments on inorganic polymers synthesis and applications. *Ceram. Int.* **42**, 15142–15159 (2016).
44. Peter Olusakin Oladoye, Timothy Oladiran Ajiboye, Elizabeth Oyinkansola Omotola, Olusola Joel Oyewola, Methylene blue dye: Toxicity and potential elimination technology from wastewater, *Results in Engineering*, Volume 16, 100678, ISSN 2590–1230. (2022).
45. Lagergren, S. K. About the theory of so-called adsorption of soluble substances. *Sven. Vetenskapsakad. Handlingar*. **24**, 1–39 (1898).
46. Farhan, A. M., Salem, N. M., Ahmad, A. L. & Awwad, A. M. Kinetic, equilibrium and thermodynamic studies of the biosorption of heavy metals by *Ceratonia siliqua* bark. *Am. J. Chem.* **2**, 335–342 (2012).
47. Abdi, O. & Kazemi, M. A review study of biosorption of heavy metals and comparison between different biosorbents. *J. Mater. Env. Sci.* **6**, 1386–1399 (2015).
48. Khan, H. et al. Novel modelling and optimization framework for Navy Blue adsorption onto eco-friendly magnetic geopolymer composite. *Environ. Res.* **216**, 114346 (2023).
49. Ryu, G. S., Lee, Y. B., Koh, K. T. & Chung, Y. S. Mechanical properties of fly ash-based geopolymer concrete with alkaline activators. *Constr. Build. Mater.* **47**, 409–418 (2013).
50. El Alouani, M., Alehyen, S., El Achouri, M. & Taibi, M. Preparation, characterization, and application of metakaolin-based geopolymer for removal of methylene blue from aqueous solution. *J. Chem.* **2019**, 1–14 (2019).
51. Jin, M., Zheng, Z., Sun, Y., Chen, L. & Jin, Z. Resistance of metakaolin-MSWI fly ash based geopolymer to acid and 12 *Journal of Chemistry alkaline environments. J. Non-Cryst. Solids* **450**, 116–122 (2016).
52. Maged, A., Abu El-Magd, S. A., Radwan, A. E., Kharbush, S. & Zamzam, S. Evaluation insight into Abu Zenima clay deposits as a prospective raw material source for ceramics industry: Remote sensing and characterization. *Sci. Rep.* **13**, 1–16 (2023).
53. Nmiri, A., Yazoghli, O., Duc, M., Hamdi, N. & Srasra, E. Temperature effect on mechanical and physical properties of Na or K alkaline silicate activated metakaolin-based geopolymers. *Italian J. Eng. Geol. Environ.* **1**, 5–15. <https://doi.org/10.4408/IJEGE.2016-01.O-01> (2016).
54. Belmokhtar, N., Ammari, M., Brigui, J. & Ben allal, L., Comparison of the microstructure and the compressive strength of two geopolymers derived from Metakaolin and an industrial sludge. *Construct. Build. Mater.* **146**, 621–629. <https://doi.org/10.1016/j.conbuildmat.2017.04.127> (2017).
55. El Alouani, M., Alehyen, S., Aouan, B., Mabrouki, J. & Saufi, H. Application of mesoporous fly ash as a low-cost adsorbent for effective removal and immobilization of hazardous pollutants in aqueous environments. *Model. Earth Syst. Environ.* <https://doi.org/10.1007/s40808-023-01715-4> (2023).
56. Gómez-Casero, M.A., De Dios-Arana, C., Bueno-Rodríguez, J.S., Pérez-Villarejo, L., Eliche-Quesada, D., Physical, mechanical and thermal properties of metakaolin-fly ash geopolymers. *Sustainable Chemistry and Pharmacy* **26**, 100620. <https://doi.org/10.1016/j.scp.2022.100620>. (2022).
57. Merabtene, M., Kacimi, L. & Clastres, P. Elaboration of geopolymer binders from poor kaolin and dam sludge waste. *Heliyon* **5**, e01938. <https://doi.org/10.1016/j.heliyon.2019.e01938> (2019).
58. Ozer, I. & Soyer-Uzun, S. Relations between the structural characteristics and compressive strength in metakaolin based geopolymers with different molar Si/Al ratios. *Ceram. Int.* **41**(8), 10192–10198 (2015).

59. Bhaskar, J. Saikia, Gopalakrishnarao Parthasarathy, Fourier Transform Infrared Spectroscopic Characterization of Kaolinite from Assam and Meghalaya Northeastern India. *J. Mod. Phys.* **1**, 206–210. <https://doi.org/10.4236/jmp.2010.14031> (2010).
60. Salam, M. A. et al. Insight into the role of the zeolitization process in enhancing the adsorption performance of kaolinite/diatomite geopolymer for effective retention of Sr (II) ions; batch and column studies. *J. Environ. Manage.* **294**, 112984 (2021).
61. Duxson, P., Mallicoat, S. W., Lukey, G. C., Kriven, W. M. & van Deventer, J. S. J. The effect of alkali and Si/Al ratio on the development of mechanical properties of metakaolin-based geopolymers Colloids Surfaces. *A Physicochem. Eng. Asp.* **292**, 8–20 (2007).
62. Abutaleb, A., Imran, M., Zouli, N., A. H. Khan, A. H., Hussain, S., M. A. Ali, M. A. et al., Fe<sub>3</sub>O<sub>4</sub>-multiwalled carbon nanotubes-bentonite as adsorbent for removal of methylene blue from aqueous solutions, *Chemosphere*, 316, 137824. (2023).
63. R.M. Novais, G. Ascens'ao, D.M. Tobaldi, M.P. Seabra, J.A. Labrincha, Biomass fly ash geopolymer monoliths for effective methylene blue removal from wastewaters, *J. Clean. Prod.* **171**, 783–794, [10.1016/j.jclepro.2017.10.078](https://doi.org/10.1016/j.jclepro.2017.10.078), (2018).
64. Novais, R. M. et al. Synthesis of porous biomass fly ash-based geopolymer spheres for efficient removal of methylene blue from wastewaters. *J. Clean. Prod.* **207**, 350–362. <https://doi.org/10.1016/j.jclepro.2018.09.265> (2019).
65. F. M. Maingi, H. M. Mbuvi, M. M. Ng'ang'a, H. Mwangi, Adsorption Kinetics and Isotherms of Methylene Blue by Geopolymers Derived from Common Clay and Rice Husk Ash, *Sci & Acad Pub. Jou*, **7**(4), 87–97. (2017).
66. Khoa Dang Nguyen, Trang Tran Thu, Anh Thi Hoang Tran, Oanh Thi Kim Le, Suresh Sagadevan, and Noor Haida Mohd Kaus, Effect of Red Mud and Rice Husk Ash-Based Geopolymer Composites on the Adsorption of Methylene Blue Dye in Aqueous Solution for Wastewater Treatment, *ACS Omega*, **8** (44), 41258–41272. (2023).
67. Lian, L. & Li ping G., Guo, C., Adsorption of Congo red from aqueous solutions onto Ca- bentonite. *J. Hazard. Mater* **161**(1), 126–131 (2009).
68. Thanh Phu Le, Huynh Vu Thanh Luong, Hoang Ngoan Nguyen, Thi Kim Thu Pham, Tran Lan Trinh Le, Thi Bich Quyen Tran, Truong Ngoc Mai Ngo, Insight into adsorption-desorption of methylene blue in water using zeolite NaY: Kinetic, isotherm and thermodynamic approaches. *Results Surfaces Interfaces* **16**, 100281 (2024).
69. Shakoor, S. & Nasar, A. Removal of methylene blue dye from artificially contaminated water using citrus limetta peel waste as a very low-cost adsorbent. *J. Taiwan Inst. Chem. Eng.* **66**, 154–163 (2016).
70. Baraka, A. Adsorptive removal of tartrazine and methylene blue from wastewater using melamine-formaldehyde-tartaric acid resin (and a discussion about pseudo second order model). *Desalin. Water Treat.* **44**(1–3), 128–141 (2012).

## Author contributions

Khaled Elewa did all the experimental work under supervision of Nabil A. Abdullah and A.F Tawfic Khaled Elewa analysed the obtained results with Nabil A. Abdullah and A.F Tawfic The manuscript was edited and reviewed by Nabil M. Nagy and Mostafa Tarek.

## Funding

Open access funding provided by The Science, Technology & Innovation Funding Authority (STDF) in cooperation with The Egyptian Knowledge Bank (EKB).

## Declarations

## Competing interests

The authors declare no competing interests.

## Ethical approval

This article doesn't contain any studies involving animals performed by any authors, also this article does not contain any studies involving human participating performed by any of the authors.

## Consent for publication

All authors have read and agreed to the published version of the manuscript.

## Consent to participate

All authors agree to participate in the published version of the manuscript

## Additional information

**Correspondence** and requests for materials should be addressed to A.F.T.

**Reprints and permissions information** is available at [www.nature.com/reprints](http://www.nature.com/reprints).

**Publisher's note** Springer Nature remains neutral with regard to jurisdictional claims in published maps and institutional affiliations.

**Open Access** This article is licensed under a Creative Commons Attribution 4.0 International License, which permits use, sharing, adaptation, distribution and reproduction in any medium or format, as long as you give appropriate credit to the original author(s) and the source, provide a link to the Creative Commons licence, and indicate if changes were made. The images or other third party material in this article are included in the article's Creative Commons licence, unless indicated otherwise in a credit line to the material. If material is not included in the article's Creative Commons licence and your intended use is not permitted by statutory regulation or exceeds the permitted use, you will need to obtain permission directly from the copyright holder. To view a copy of this licence, visit <http://creativecommons.org/licenses/by/4.0/>.

© The Author(s) 2025